JPIS
Journal of Periodontal & Implant Science

Research Article
Implant Science

Check for updates

Impact of lattice versus solid structure of 3D-printed multiroot dental implants using Ti-6Al-4V: a preclinical pilot study

Jungwon Lee [1,2], **Ling Li** [1], **Hyun-Young Song** [1], **Min-Jung Son** [1], **Yong-Moo Lee** [1,*], **Ki-Tae Koo** [1,*]

[1]Department of Periodontology and Dental Research Institute, School of Dentistry, Seoul National University, Seoul, Korea
[2]One-Stop Specialty Center, Seoul National University Dental Hospital, Seoul, Korea

OPEN ACCESS

*Correspondence:
Yong-Moo Lee
Department of Periodontology and Dental Research Institute, School of Dentistry, Seoul National University, 101 Daehak-ro, Jongno-gu, Seoul 03080, Korea.
Email: ymlee@snu.ac.kr
Tel: +82-2-2072-3024
Fax: +82-2-744-0051

Ki-Tae Koo
Department of Periodontology and Dental Research Institute, School of Dentistry, Seoul National University, 101 Daehak-ro, Jongno-gu, Seoul 03080, Korea.
Email: periokoo@snu.ac.kr
Tel: +82-2-2072-0108
Fax: +82-2-744-0051

ORCID iDs
Jungwon Lee
https://orcid.org/0000-0002-5508-442X
Ling Li
https://orcid.org/0000-0002-8258-5430

ABSTRACT

Purpose: Various studies have investigated 3-dimensional (3D)-printed implants using Ti-6Al-4V powder; however, multi-root 3D-printed implants have not been fully investigated. The purpose of this study was to explore the stability of multirooted 3D-printed implants with lattice and solid structures. The secondary outcomes were comparisons between the 2 types of 3D-printed implants in micro-computed tomographic and histological analyses.
Methods: Lattice- and solid-type 3D-printed implants for the left and right mandibular third premolars in beagle dogs were fabricated. Four implants in each group were placed immediately following tooth extraction. Implant stability measurement and periapical X-rays were performed every 2 weeks for 12 weeks. Peri-implant bone volume/tissue volume (BV/TV) and bone mineral density (BMD) were measured by micro-computed tomography. Bone-to-implant contact (BIC) and bone area fraction occupancy (BAFO) were measured in histomorphometric analyses.
Results: All 4 lattice-type 3D-printed implants survived. Three solid-type 3D-printed implants were removed before the planned sacrifice date due to implant mobility. A slight, gradual increase in implant stability values from implant surgery to 4 weeks after surgery was observed in the lattice-type 3D-printed implants. The marginal bone change of the surviving solid-type 3D-printed implant was approximately 5 mm, whereas the value was approximately 2 mm in the lattice-type 3D-printed implants. BV/TV and BMD in the lattice type 3D-printed implants were similar to those in the surviving solid-type implant. However, BIC and BAFO were lower in the surviving solid-type 3D-printed implant than in the lattice-type 3D-printed implants.
Conclusions: Within the limits of this preclinical study, 3D-printed implants of double-rooted teeth showed high primary stability. However, 3D-printed implants with interlocking structures such as lattices might provide high secondary stability and successful osseointegration.

Keywords: Dental implant; Osseointegration; 3D printing

Generated by xmlinkpress

Hyun-Young Song
https://orcid.org/0000-0002-4124-4218
Min-Jung Son
https://orcid.org/0000-0002-1658-7198
Yong-Moo Lee
https://orcid.org/0000-0002-5619-3847
Ki-Tae Koo
https://orcid.org/0000-0002-9809-2630

Conflict of Interest

No potential conflict of interest relevant to this article was reported.

Author Contributions

Conceptualization: Jungwon Lee, Ki-Tae Koo; Formal analysis: Yong-Moo Lee, Ki-Tae Koo; Investigation: Jungwon Lee, Ling Li, Hyun-Young Song, Min-Jung Son; Methodology: Jungwon Lee, Ling Li, Hyun-Young Song, Min-Jung Son; Project administration: Ki-Tae Koo; Writing - original draft: Jungwon Lee, Ling Li, Hyun-Young Song, Min-Jung Son; Writing - review & editing: Yong-Moo Lee, Ki-Tae Koo.

INTRODUCTION

The manifold shapes of natural teeth provide complex odontostomatognathic functions and a unique biomechanical masticatory system. A key fact is that anterior teeth have a single root, while posterior teeth have multiple roots [1,2], which corresponds to greater occlusal forces [3]. In fact, long-term retrospective studies in clinical practice have reported that implant component fractures occurred more frequently in the posterior region than in the anterior region [4]. Therefore, the replacement of missing posterior teeth with multiroot dental implants might satisfy biomechanical requirements for function, enabling the personalization of tooth forms.

Despite the substantially successful osseointegration of immediate conventional thread-type dental implants in the posterior region in well-selected cases [5], the unavoidable gap between the implant and the extraction socket due to 3-dimensional (3D) discrepancies could be remarkable compared to those in the anterior region. Several studies have suggested regenerative procedures in immediate implant placement to overcome this problem [6,7]. However, a regenerative procedure incurs additional costs and increases the operation time, which places a burden on the patient.

A novel implant with multiple roots in the posterior region could provide an alternative to reduce the mechanical complications of implants or regenerative procedures. The development of digital technologies, including cone-beam computed tomography (CT) and intraoral scanning, has enabled the creation of elaborate 3D-printed individual implants [8,9]. In addition, noticeable advances have been made in additive manufacturing processes (i.e., 3D printing technology) in dentistry. Among the various metal 3D printing processes, direct metal laser sintering (DMLS) is considered to be a time-saving and cost-effective process in fabricating 3D metal structures [10]. Several studies have demonstrated the successful manufacture of 3D-printed dental implants with the DMLS technique, showing biocompatibility *in vivo* [11-13].

The low feasibility and inconvenience of immediate placement with thread-type implants in the posterior region is another issue. Although various surgical techniques have been suggested to overcome difficulties and inconveniences in immediate placement [14-17], it remains clinically difficult to place an implant in a multiroot area. 3D-printed root analog implants can contribute to strategies for immediate implant placement for multirooted teeth with minimally invasive surgery.

In clinical situations, poor bone quality is frequently encountered in the surgical site when performing immediate implant placement. To increase the likelihood of implant success, implant stability should be guaranteed before implant prosthesis delivery. Various studies have demonstrated that implant macrodesign might affect both primary and secondary stability [18,19]. Increased implant surfaces with interlocking structures, such as lattice structures, might be beneficial for primary and secondary stability. It is necessary to examine the effects of modifying the macrodesign of 3D-printed implants.

Our previous studies [12,13] established the possibility of the clinical application of a single-root 3D-printed implant. However, the feasibility of multiroot 3D-printed implants has not yet been confirmed. In addition, since grade 2 powder was used in previous studies, mechanical limitations prevented its use in the posterior region. Therefore, it would

be valuable to explore 3D-printed implants using Ti-6Al-4V powder, which is known to have high strength and fracture toughness compared with pure titanium, as well as good biocompatibility and corrosion resistance for biomedical devices [20,21].

The purpose of this study was to explore the stability of a multirooted 3D-printed implant using Ti-6Al-4V powder with lattice and solid structures. The secondary outcomes were comparisons between the 2 types of 3D-printed implants in micro-computed tomographic and histological analyses.

MATERIALS AND METHODS

The animal experiment was approved by the Institutional Animal Care and Use Committee of Seoul National University (IACUC; approval No. SNU-200323-6-2) and performed according to the principles of the 3 R's (replacement, reduction, and refinement) and 2 main laws in Korea: the Animal Protection Act established by the Ministry of Agriculture Food and Rural Affairs and the Laboratory Animal Act established by the Ministry of Food and Drug Safety. The manuscript was written according to the Animal Research: Reporting of In Vivo Experiments (ARRIVE) guidelines. The overall timeline of this study is summarized in **Figure 1A**.
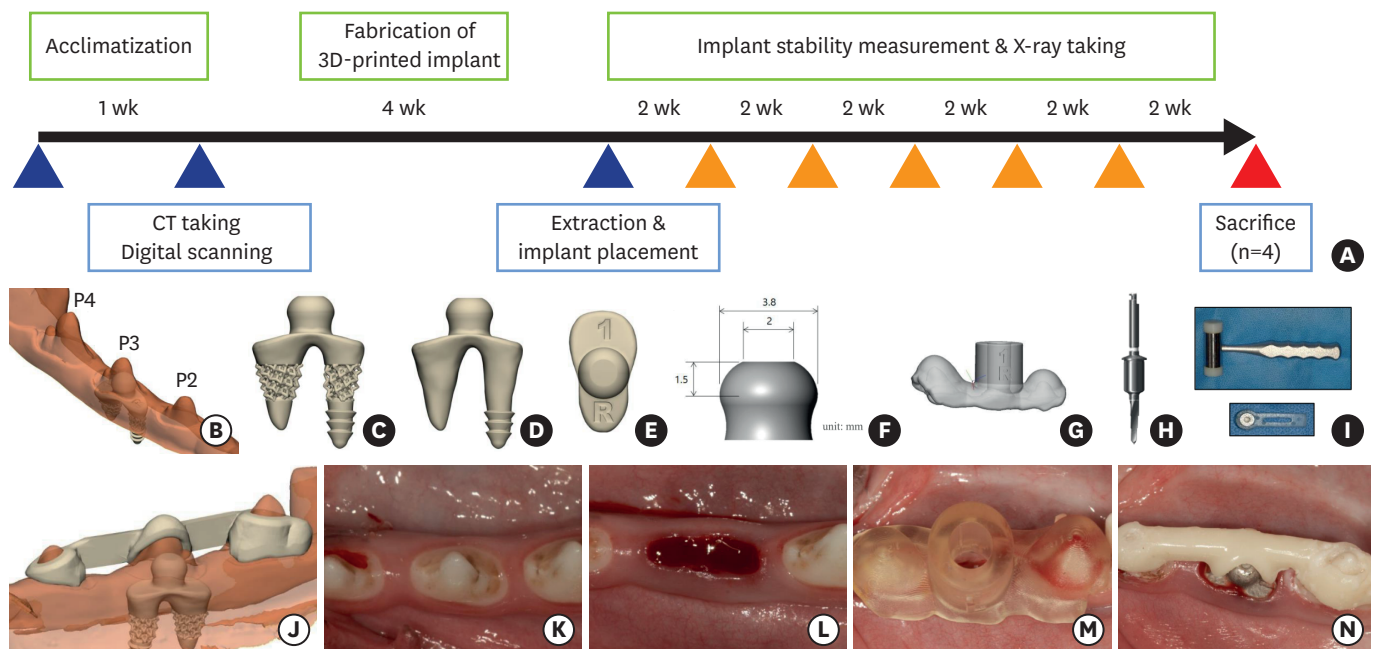
Figure 1. Overview of this experiment. (A) Timeline of the study. (B) Computed tomography and intraoral scan data were superimposed, and a 3D-printed implant was planned with software. (C) Side view of a lattice-type 3D-printed implant. (D) Side view of a solid-type 3D-printed implant. (E) Top view of a 3D-printed implant. The number indicates the animal identification, and the letter indicates the location, distinguishing right (R) and left (L). (F) Abutment of 3D-printed implants. All 3D-printed implants had identical abutment sizes and shapes. (G) Surgical guide for drilling at the mesial root site. (H) A 2.3×10 mm guide drill was used for mesial root drilling. (I) Mallet and mallet receiver. In order to place 3D-printed implant with proper direction, malleting was performed to the mallet receiver that connected the abutment of 3D-printed implants. (J) Buccal view of a protective cap. (K) Clinical photograph before surgery. (L) Clinical photograph after tooth extraction. (M) A surgical guide was applied to the surgical site. (N) A protective cap was attached to the adjacent teeth.
3D: 3-dimensional.

Fabrication of 3D-printed implants

Four male beagle dogs approximately 1 year old, weighing approximately 10–12 kg, were used for this study. CT datasets of the mandible, including teeth, were acquired using a CT scanner (GE, Boston, MA, USA). The CT datasets were transferred in the Digital Imaging and Communications in Medicine format to 3D reconstruction software (Materialise, Leuven, Belgium). The left and right sides of mandibular third premolars were virtually extracted and isolated as a stereolithography (STL) file with the software. The STL file was transferred to software (Materialise) to make virtual 3D multiroot implants (**Figure 1B**). The structures of double root implants were the groove at the mesial root at the apex area and lattice at the middle area of the root (lattice type, **Figure 1C**) and groove at the apex of the mesial root and no lattice at the other root surface (solid type, **Figure 1D**). The inner depth and external protrusion of the lattice structure were each 0.3 mm. To obtain primary stability, the mesial root of the 3D-printed implant was fabricated to be 2 mm longer than the corresponding teeth with a groove. The implants were marked in the upper area using numbers and letters to identify animals and locations (**Figure 1E**). The dimensions of the roots of the 3D-printed implants were different for each tooth; however, the abutment was manufactured with a constant size (**Figure 1F**). The 3D-printed implants were sterilized using gamma-ray irradiation, which is a short-wavelength light emitted from the cobalt-60 (^{60}Co) radioactive isotope according to ISO11137, following large-grit sandblasting and acid-etching (SLA) surface treatment according to a previous study [13]. To perform osteotomy at the mesial root at the planned site, a surgical guide (**Figure 1G**) and drill were fabricated (**Figure 1H**). To minimize the loading on the implant, a protective cap with a thickness of 1 mm was fabricated using a polymer (DG-1, Hephzibah, Inchon, Korea) (**Figure 1I and J**).

Immediate placement of 3D-printed implants

The animals were anesthetized using intravenous injections of tiletamine/zolazepam (5 mg/kg, Virbac, Carros, France), xylazine (2.3 mg/kg, Bayer Korea, Ansan, Korea), and 0.05 mg/kg atropine sulfate during the surgical procedures. All procedures related to general anesthesia were performed by a veterinarian. Complementary local anesthesia was conducted at the mandibular third premolar area with 2% lidocaine HCl with epinephrine (1:1,000,000, Huons, Seongnam, Korea). The third premolars were hemisectioned in the buccolingual direction of the teeth with a diamond fissure bur and atraumatically extracted using an elevator and forceps without flap reflection (**Figure 1E and F**). The apical portion of the extraction socket was prepared at the mesial root site to place the 3D-printed implants, which were 2 mm longer than the corresponding teeth of the mesial root using a 2.3-mm-diameter drill with a motor-driven handpiece (EXPERTsurg™ LUX, KaVo, Warthausen, Germany) (**Figure 1G**). One of the 2 types of 3D-printed implant (lattice type or solid type) was randomly placed at each of the left or right sides of the mandible according to a random sequence generated before surgery. The 3D-printed implant heads were directly tapped using a surgical mallet. The protective cap was attached to the adjacent teeth using resin-modified glass ionomer cement (GC FujiCEM®2, Tokyo, Japan) (**Figure 1**).

Postoperative care

To assuage postoperative pain and inflammation, an antibiotic (cefazoline, 20 mg/kg, Chongkundang Pharm., Seoul, Korea) and analgesic (tramadol hydrochloride, 5 mg/kg, Samsung Pharm., Hwaseong, Korea) were intravenously injected after surgery. Subsequently, antibiotics (Amoxicillin, 500 mg, Chongkundang Pharm.) and analgesics (Ibuprofen 400 mg, Daewoong Pharm., Seoul, Korea) were administered by mixing with the animals' diet for 3 days following the surgery. A soft diet was provided for 1 month after surgery to avoid
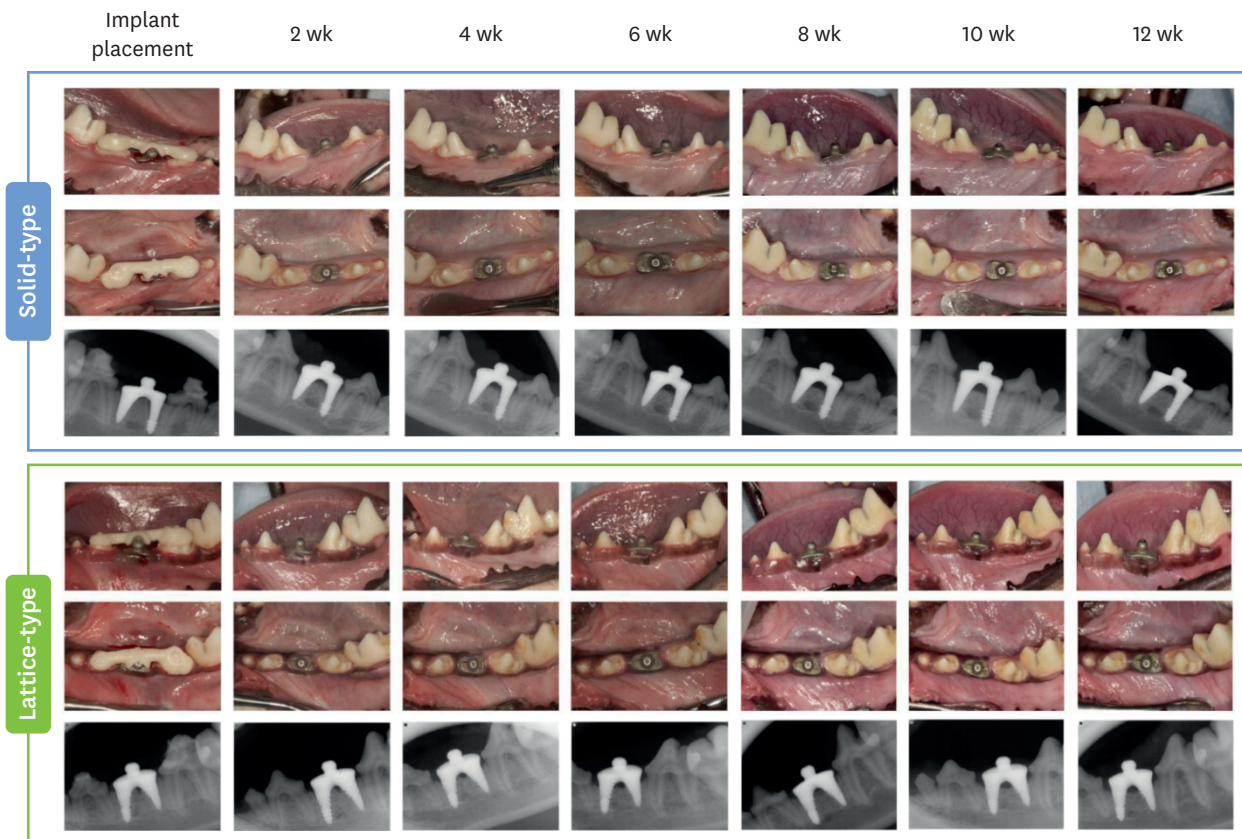
Figure 2. Clinical and radiographic photograph of solid-type and lattice-type 3D-printed implants. All protective caps were removed 2 weeks after implant placement for plaque control and implant stability measurements.
3D: 3-dimensional.

any mechanical interference that might delay wound healing. The surgical sites were checked every 2 weeks and rinsed with 0.12% chlorhexidine gluconate solution (Hexamedine®, Bukwang Pharm., Seoul, Korea) (**Figure 2A**).

### Implant stability measurements

According to a previous study, damping capacity analysis (Anycheck, Neobiotech, Seoul, Korea) was performed to measure implant stability [12]. Each implant was measured 5 times on the buccal side, and the average value of the measurements was considered representative for each implant.

Marginal bone changes

Intraoral periapical radiographs were taken to investigate marginal bone changes. The marginal bone changes were measured at the mesial, middle, and distal sites of each implant. Marginal bone loss was calculated using the ratio between the actual distance and the distance on the radiograph, following the method suggested in a previous study (**Figure 3A**) [22]. The difference in the marginal bone level between implant placement and 12 weeks after implant placement was compared.

Micro-CT analyses

At 12 weeks after implant placement, the animals were sacrificed by carotid injection with potassium chloride (75 mg/kg, Jeil Pharm., Daegu, Korea). Block biopsies including the
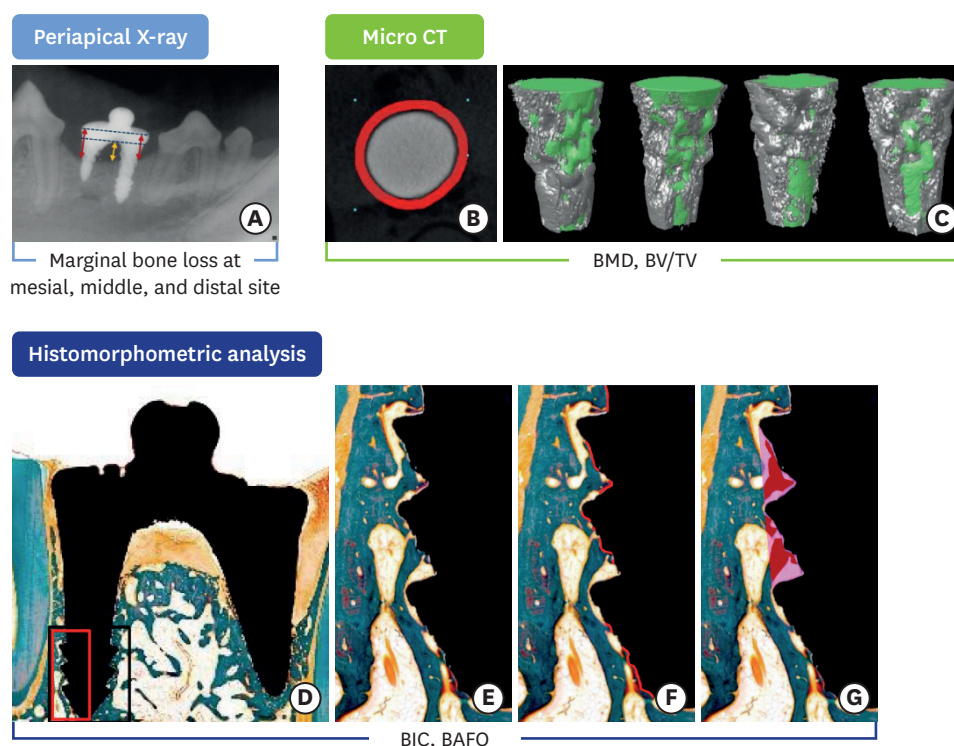
Figure 3. Schematic diagram of data analyses. (A) Marginal bone loss at the mesial, middle, and distal sites was measured with periapical X-ray examinations. (B) The VOI was set to a 190-μm circular band stretching 60–2,250 μm from the implant surface of each root. The vertical dimension was limited from 1 mm above the fixture apex to 4 mm. (C) Gray and green areas indicate the VOI and 3D-printed implants, respectively. BMD and BV/TV were measured in the gray area. (D-G) Within the region of interest, BIC at each root of the implant and BAFO at the mesial root, which had a groove, were measured.
CT: computed tomography, BMD: bone mineral density, BV/TV: bone volume/tissue volume, 3D: 3-dimensional, BIC: bone-to-implant contact, BAFO: bone area fraction occupancy, VOI: volume of interest.

implant placement sites were obtained for histologic observations and histomorphometric analyses. Before the histological preparation, the blocks obtained from each experimental site were prepared for micro-CT. The blocks were scanned at a 13.3-μm resolution, 60 kV, and 167 μA using a 0.5-mm aluminum filter and a 3-dimensional micro-CT machine (SkyScan® 1172, SkyScan, Aartselaar, Belgium). Two-dimensional images were saved as .bmp files (2,240×2,240 pixels), and then the axes of the sagittal and transverse images were reoriented using image analysis software (DataViewer 1.5.2.4 64-bit version, Bruker microCT, Skyscan, Kontich, Belgium).

The volume of interest (VOI) was set to a 190-μm circular band stretching 60–2,250 μm from the implant surface of each root to discriminate the effects of metal artifacts from the surface in accordance with a previous study (**Figure 3B**) [23]. The vertical dimension was limited from 1 mm to 4 mm above the fixture apex (**Figure 3C**). Within the VOI, bone mineral density and the bone volume/tissue volume ratio (BV/TV) were measured using software (CTAn, Bruker-CT, Kontich, Belgium). The 8-bit grayscale values were set to range from 30 to 80 in order to identify bone tissue.

Histological preparation

The specimens were maintained in a fixative solution containing 10% neutral formalin buffer

for 1 week and subsequently dehydrated in increasing grades of ethanol solution. Thereafter, the samples were embedded in methacrylate (Technovit 7200, Heraeus Kulzer, Hanau, Germany) in accordance with the manufacturer's instructions. The block was sectioned in the mesiodistal direction using a diamond saw. Thereafter, the sections were ground and polished to approximately 80±5 μm and then stained with Goldner trichrome.

Histological and histomorphometric analyses

The slides were examined under a light microscope (BX51, OLYMPUS, Tokyo, Japan) connected to a CCD camera (SPOT Insight 2 Mp scientific CCD digital camera system, Diagnostic Instruments, Inc., Sterling Heights, MI, USA) and an adaptor (U-CMA3, OLYMPUS). The histological images were stored as digital image files for histomorphometric analysis. With a computer-aided slide image analysis program (CaseViewer 2.2; 3DHISTECH Ltd., Budapest, Hungary), the region of interest (ROI) was selected at the mesial and distal root of the implants from 1 mm to 4 mm above the fixture apex. Within the ROI, bone-to-implant contact (BIC) at each root of the implant and bone area fraction occupancy (BAFO) at the mesial root, which had a groove, were measured as described in previous studies (**Figure 2D-G**) [13]. Histomorphometric measurements were performed twice by an experienced examiner using image analysis software.

Statistical analysis

A sample size calculation was not performed due to the pilot nature of the study. Descriptive statistical analyses were performed due to the missing data for the solid type of 3D printed implants. All data for the lattice type of 3D printed implants are presented as the mean±SD, whereas only measured data for solid-type 3D-printed implants are presented.

RESULTS

Clinical observations

All 4 lattice-type 3D-printed implants survived. Two solid-type 3D-printed implants were removed at 2 weeks and another at 4 weeks due to mobility and signs of peri-implant soft tissue inflammation, including redness and swelling. All protective caps were removed 2 weeks after implant placement for plaque control and implant stability measurement.

Implant stability measurements and marginal bone loss changes

The implant stability value of the lattice-type 3D-printed implants was 69.95±0.97 at implant surgery, increased to approximately 76 at 4 weeks, and then remained constant until 12 weeks (**Table 1**). The implant stability value of the solid-type 3D-printed implants was 70.55±0.81 at implant placement; however, it decreased to 45.00±18.05 at 2 weeks (**Table 1**). Two implants at 2 weeks and 1 implant at 4 weeks were removed due to implant mobility after measuring implant stability. The surviving solid-type implant had an implant stability value of 68.4 at 12 weeks.

Marginal bone changes

The marginal bone changes in the mesial, middle, and distal sites of the solid-type 3D-printed implants were larger than those of the lattice-type 3D-printed implants (**Figure 4**). The differences in marginal bone changes between the solid- and lattice-type 3D-printed implants were approximately 3 mm. Marginal bone loss was more pronounced in the solid-type 3D-printed implants; however, marginal bone loss of approximately 2 mm was also observed in the lattice-type 3D-printed implants.

Table 1. Implant stability values during the study period

Type	Animal	Surgery	2 wk	4 wk	6 wk	8 wk	10 wk	12 wk
Lattice type of 3D-printed implants	#1	69	71	75.2	75	75.2	73.2	74
	#2	69.4	67.4	75.8	79.2	80.4	79.8	81
	#3	70.2	70.8	74	76	75.2	75.8	77.8
	#4	71.2	79	78.4	76.2	75	77.2	77
	Mean±SD	69.95±0.97	72.05±4.92	75.85±1.86	76.6±1.81	76.45±2.63	76.5±2.75	77.45±2.87
Solid type of 3D-printed implants	#1	71	43[a]	NA	NA	NA	NA	NA
	#2	71.2	42.8	25[a]	NA	NA	NA	NA
	#3	70.6	25.2[a]	NA	NA	NA	NA	NA
	#4	69.4	69	68.8	68.8	70.4	70	68.4
	Mean±SD	70.55±0.81	45.00±18.05	-	-	-	-	-

Mean±SD were calculated only when all implants were survived.
3D: 3-dimensional, NA: not available.
[a]Removed implant after measuring implant stability due to implant mobility at that time.
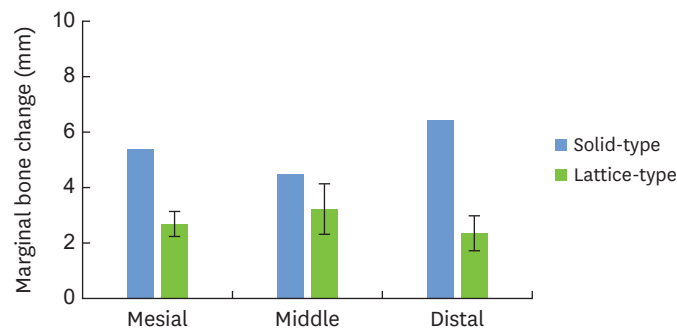
Figure 4. Marginal bone change between baseline and 12 weeks of observation. The mean and SD were calculated only in lattice-type 3D-printed implants due to the missing data for solid-type 3D-printed implants.
3D: 3-dimensional.

Micro-CT analyses

Micro-CT was performed on 1 solid-type implant sample and 4 lattice-type implant samples (**Figure 5A**). The mean BV/TV value measured at the mesial and distal root of the surviving solid-type implant was 60.76%. The BV/TV values in the lattice-type 3D-printed implants were 53.99%±9.98% (**Table 2**). The BV/TV at the mesial root (with a groove structure) and distal root (without a groove structure) of the lattice-type 3D-printed implants were 62.27%±5.71% and 45.71%±4.12%, respectively, showing statistically significant differences (P=0.029).

The mean BMD measured at the mesial and distal root of the surviving solid-type implant was 1.25 g·cm^{-3}. The mean BMD in the lattice-type 3D-printed implants was 1.06±0.24 g·cm^{-3} (**Table 2**). The BMD values in the mesial root (with a groove structure) and distal root (without a groove structure) of the lattice-type 3D-printed implants were 0.93±0.17 g·cm^{-3} and 1.19±0.25 g·cm^{-3}, respectively, showing no statistically significant difference (P=0.200).

Table 2. Micro-CT and histomorphometric analyses

| Parameters	Lattice type of 3D-printed implants		Solid type of 3D-printed implants	
BV/TV (%)	4	53.99±9.98	1	60.76
BMD (g·cm^{-3})	4	1.06±0.24	1	1.25
BIC (%)	4	78.12±10.96	1	53.67
BAFO (%)	4	62.58±5.51	1	52.26

Data are shown as number or mean±SD.
BV/TV and BMD were measured with micro-CT.
BIC at each root of the implant and BAFO at the mesial root, which has a groove, were measured in histomorphometric analysis.
CT: computed tomography, 3D: 3-dimensional, BV/TV: bone volume/tissue volume, BMD: bone mineral density, BIC: bone-to-implant contact, BAFO: bone area fraction occupancy.
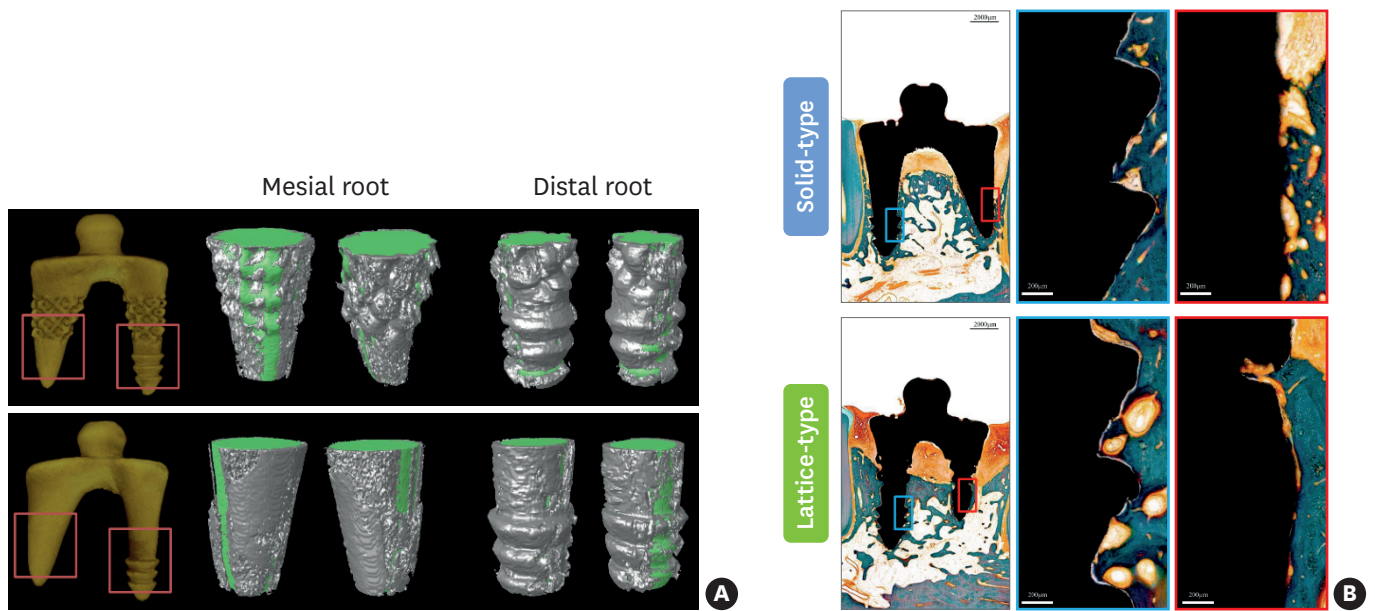
Figure 5. Representative micro-computed tomography (A) and histologic view (B). The blue and red boxes in the histologic view (B) show the area of the mesial root (with a groove structure) and distal root (without a groove structure), respectively.

Histological observations

The 3 failed solid-type 3D-printed implants could not be subjected to histological and histomorphometric analysis. All surviving solid- and lattice-type 3D-printed implants showed no specific inflammation signs (**Figure 5B**). The marginal bone loss pattern, including the furcation area, could be observed in both types of 3D-printed implants, with differences only in degree.

Histomorphometric analyses

The BIC in the lattice-type 3D-printed implants was 78.12%±10.96% (**Table 2**). The BIC of the surviving solid-type implant was 53.67%. The BAFO value in the lattice-type 3D-printed implants was 62.58%±5.51%. The BAFO of the surviving solid-type implant was 52.26%. Although a statistical analysis was not performed, the values of BIC and BAFO were lower in the solid-type 3D-printed implant than in the lattice-type 3D-printed implants.

DISCUSSION

This study comparing solid- and lattice-type 3D-printed implants using Ti-6Al-4V powder showed that (i) lattice-type 3D-printed implants presented higher secondary implant stability values and survival than solid-type 3D-printed implants; (ii) lattice-type 3D-printed implants had comparable BV/TV and BMD values to those of the surviving solid-type 3D-printed implant in micro-CT analyses; and (iii) lattice-type 3D-printed implants presented higher BIC and BAFO values than the surviving solid-type 3D-printed implant in histomorphometric analyses.

In recent years, 3D printing technologies have been widely applied in dentistry. The additive manufacturing process makes it possible to fabricate individualized designs. The possibility of applying 3D-printed implants has been investigated with macrodesign modifications and surface treatments [12,13]. However, there is limited evidence that multiroot implants can

be made using 3D-printing technology and placed. This study demonstrated that lattice-type 3D-printed implants with macroretention structures showed high implant survival and implant stability, suggesting the potential for individualized implants.

A possible complication in the process of custom-made 3D-printed implant placement is fracture of the buccal bone plate [24]. The 3D-printed implants were manufactured to reflect the appearance of each tooth as much as possible, with a decrease of approximately 0.3 mm from the extraction socket to prevent fracture of the cortical bone plate and undercut area and a length of 2 mm at the mesial root (with a groove structure) to obtain primary stability. This discrepancy between the extraction socket and 3D-printed implants allowed the implants to be placed in a different position from the planned position. In addition, correction of the location after implant placement is difficult due to the implant placement method (i.e., the malleting technique); it is thus imperative to perform accurate drilling. Therefore, a surgical guide was used in this study to drill accurately at the mesial root site. However, unlike recently used surgical guides, this guide could not be used to establish the placement location and/or depth. The placement procedure needs to be supplemented in future studies.

Achieving primary implant stability in immediate implant placement has been considered one of the pivotal factors for successful implants [25]. From this point of view, all solid-type and lattice-type 3D-printed implants fulfilled the criteria. However, 3 of the 4 solid-type 3D-printed implants failed to achieve secondary implant stability, resulting in their removal from the placed sites. This result might be because there are few structures that can undergo interlocking during the wound healing process. The significance of the macroretention design in this study is consistent with a previous study demonstrating that all root analog zirconia implants without macroretention design failed, whereas those with macroretention design showed a 92% survival rate [26]. Although the solid-type 3D-printed implants had a groove design at the medial root, it seems that additional interlocking or macroretention structures are needed for secondary stability.

A stability dip is observed during the wound healing period when primary implant stability decreases, whereas secondary implant stability gradually increases with some delay [27]. In this study, the implant stability dip was not clearly observed. It is thought that solid-type 3D-printed implants failed before the secondary implant stability increased. In the case of the lattice-type implants, since the implant stability value was measured every two weeks, it is possible that the stability dip occurred before 2 weeks after the implant placement and was therefore not detected. A previous study reported that the implant stability dip appeared most clearly 1 week after implantation [28]. In addition, most 3D-printed implants in this study showed implant stability values of 70 or higher, and stability dips tended not to appear clearly in examples with high primary implant stability.

The marginal bone change of solid-type 3D-printed implants was higher than that of lattice-type 3D-printed implants. In addition, the 3 failed implants showed rapid peri-implant bone loss patterns. The rapid bone loss occurred within the first 4 weeks following implant placement, which might be related to implant stability. These results can also be understood in the same context as implant stability, as discussed above. The macrodesign of the implant is likely to have been the factor that affected its secondary stability because both types of 3D-printed implants were treated with the same surface modification of SLA. Mechanically interlocking stability with a macroretention design might be maintained for a period of time to achieve sufficient osseointegration, especially if the abutment is exposed to the oral environment.

It should be noted that the lattice-type 3D-printed implants showed 2 mm of marginal bone loss, although marginal bone loss was immaterial compared to that in the solid-type 3D-printed implants. This result is similar to the outcomes of previous studies related to immediate implant placement [29,30]. From this result, when performing immediate implant placement, approximately 2 mm of crestal bone loss should be expected regardless of whether the implant is a conventional threaded type implant or a 3D-printed root analog form implant. In future studies, the expectation of crestal bone loss following immediate implant placement should be reflected in the 3D-printed implant macrodesign.

In the micro-CT analysis, BV/TV was higher in lattice-type 3D-printed implants than in solid-type 3D-printed implants. However, the surviving solid-type 3D-printed implant showed a similar value to those of the lattice-type 3D-printed implants. A similar pattern was observed in BMD. BIC and BAFO in the histomorphometric analyses showed higher values in the solid-type implants than in the lattice-type 3D-printed implants in this study. However, the BIC and BAFO of the surviving solid-type implant were comparable to those of lattice-type implants. If the implant is kept stable until the appropriate time point, the macrodesign of a 3D-printed implant does not seem to have a significant effect on the distant peri-implant bone healing pattern. This result is consistent with a previous study in which different implant macrodesigns showed similar degrees of osseointegration [31]. From this result, it was confirmed that Ti-6Al-4V powder is a biocompatible material, and the achieving implant stability is the key factor in successfully printing 3D implants.

In this study, 3D-printed implants were not evaluated under loading conditions using prostheses. Occlusion can affect peri-implant hard tissue remodeling in response to mechanical stress. From this point of view, 3D-printed implants should be investigated under loading with implant prostheses in future studies.

Another limitation of this study is the parallel double-root design. Generally, the roots of natural teeth show divergence, distributing the occlusal force. However, the exact divergence shape could not be reflected in the 3D-printed implants used in this study due to technical difficulties in the process of implant placement. It is necessary to confirm that a parallel root shape can distribute occlusal force comparably to the divergent roots of natural teeth in the future.

Within the limitations of this preclinical study, 3D-printed implants of double-rooted teeth showed high primary stability. Furthermore, 3D-printed implants with interlocking structures such as lattices might provide high secondary stability and successful osseointegration.

REFERENCES

1. Ahmed HMA, Versiani MA, De-Deus G, Dummer PMH. A new system for classifying root and root canal morphology. Int Endod J 2017;50:761-70.
   PUBMED | CROSSREF

2. Ahmed HMA, Ibrahim N, Mohamad NS, Nambiar P, Muhammad RF, Yusoff M, et al. Application of a new system for classifying root and canal anatomy in studies involving micro-computed tomography and cone beam computed tomography: explanation and elaboration. Int Endod J 2021;54:1056-82.
   PUBMED | CROSSREF

3. Kumagai H, Suzuki T, Hamada T, Sondang P, Fujitani M, Nikawa H. Occlusal force distribution on the dental arch during various levels of clenching. J Oral Rehabil 1999;26:932-5.
   PUBMED | CROSSREF

https://doi.org/10.5051/jpis.2105720286

4. Yi Y, Koak JY, Kim SK, Lee SJ, Heo SJ. Comparison of implant component fractures in external and internal type: a 12-year retrospective study. J Adv Prosthodont 2018;10:155-62.
   PUBMED | CROSSREF

5. Ragucci GM, Elnayef B, Criado-Cámara E, Del Amo FS, Hernández-Alfaro F. Immediate implant placement in molar extraction sockets: a systematic review and meta-analysis. Int J Implant Dent 2020;6:40.
   PUBMED | CROSSREF

6. Lee J, Park D, Koo KT, Seol YJ, Lee YM. Validity of a regenerative procedure for a minor bone defect with immediate implant placement: a systematic review and meta-analysis. Acta Odontol Scand 2019;77:99-106.
   PUBMED | CROSSREF

7. Clementini M, Tiravia L, De Risi V, Vittorini Orgeas G, Mannocci A, de Sanctis M. Dimensional changes after immediate implant placement with or without simultaneous regenerative procedures: a systematic review and meta-analysis. J Clin Periodontol 2015;42:666-77.
   PUBMED | CROSSREF

8. Tack P, Victor J, Gemmel P, Annemans L. 3D-printing techniques in a medical setting: a systematic literature review. Biomed Eng Online 2016;15:115.
   PUBMED | CROSSREF

9. Lin L, Fang Y, Liao Y, Chen G, Gao C, Zhu P. 3D printing and digital processing techniques in dentistry: a review of literature. Adv Eng Mater 2019;21:1801013.
   CROSSREF

10. Mangano F, Chambrone L, van Noort R, Miller C, Hatton P, Mangano C. Direct metal laser sintering titanium dental implants: a review of the current literature. Int J Biomater 2014;2014:461534.
    PUBMED | CROSSREF

11. Witek L, Marin C, Granato R, Bonfante EA, Campos F, Bisinotto J, et al. Characterization and *in vivo* evaluation of laser sintered dental endosseous implants in dogs. J Biomed Mater Res B Appl Biomater 2012;100:1566-73.
    PUBMED | CROSSREF

12. Li L, Lee J, Amara HB, Lee JB, Lee KS, Shin SW, et al. Comparison of 3D-printed dental implants with threaded implants for osseointegration: an experimental pilot study. Materials (Basel) 2020;13:4815.
    PUBMED | CROSSREF

13. Lee J, Lee JB, Yun J, Rhyu IC, Lee YM, Lee SM, et al. The impact of surface treatment in 3-dimensional printed implants for early osseointegration: a comparison study of three different surfaces. Sci Rep 2021;11:10453.
    PUBMED | CROSSREF

14. Smith RB, Tarnow DP. Classification of molar extraction sites for immediate dental implant placement: technical note. Int J Oral Maxillofac Implants 2013;28:911-6.
    PUBMED | CROSSREF

15. Fugazzotto PA. Implant placement at the time of maxillary molar extraction: technique and report of preliminary results of 83 sites. J Periodontol 2006;77:302-9.
    PUBMED | CROSSREF

16. Fugazzotto PA. Implant placement at the time of mandibular molar extraction: description of technique and preliminary results of 341 cases. J Periodontol 2008;79:737-47.
    PUBMED | CROSSREF

17. Fugazzotto PA. Implant placement at the time of maxillary molar extraction: treatment protocols and report of results. J Periodontol 2008;79:216-23.
    PUBMED | CROSSREF

18. Lozano-Carrascal N, Salomó-Coll O, Gilabert-Cerdà M, Farré-Pagés N, Gargallo-Albiol J, Hernández-Alfaro F. Effect of implant macro-design on primary stability: a prospective clinical study. Med Oral Patol Oral Cir Bucal 2016;21:e214-21.
    PUBMED | CROSSREF

19. McCullough JJ, Klokkevold PR. The effect of implant macro-thread design on implant stability in the early post-operative period: a randomized, controlled pilot study. Clin Oral Implants Res 2017;28:1218-26.
    PUBMED | CROSSREF

20. Jang TS, Kim D, Han G, Yoon CB, Jung HD. Powder based additive manufacturing for biomedical application of titanium and its alloys: a review. Biomed Eng Lett 2020;10:505-16.
    PUBMED | CROSSREF

21. Trevisan F, Calignano F, Aversa A, Marchese G, Lombardi M, Biamino S, et al. Additive manufacturing of titanium alloys in the biomedical field: processes, properties and applications. J Appl Biomater Funct Mater 2018;16:57-67.
    PUBMED | CROSSREF

22. Lee J, Lim YJ, Kim B, Koo KT. Early loading of mandibular molar single implants: 1 year results of a randomized controlled clinical trial. Materials (Basel) 2020;13:3912.
    PUBMED | CROSSREF

23. He T, Cao C, Xu Z, Li G, Cao H, Liu X, et al. A comparison of micro-CT and histomorphometry for evaluation of osseointegration of PEO-coated titanium implants in a rat model. Sci Rep 2017;7:16270.
    PUBMED | CROSSREF

24. Kohal RJ, Hürzeler MB, Mota LF, Klaus G, Caffesse RG, Strub JR. Custom-made root analogue titanium implants placed into extraction sockets. An experimental study in monkeys. Clin Oral Implants Res 1997;8:386-92.
    PUBMED | CROSSREF

25. Koh RU, Rudek I, Wang HL. Immediate implant placement: positives and negatives. Implant Dent 2010;19:98-108.
    PUBMED | CROSSREF

26. Pirker W, Kocher A. Immediate, non-submerged, root-analogue zirconia implants placed into single-rooted extraction sockets: 2-year follow-up of a clinical study. Int J Oral Maxillofac Surg 2009;38:1127-32.
    PUBMED | CROSSREF

27. Charatchaiwanna A, Rojsiraphisa T, Aunmeungtong W, Reichart PA, Khongkhunthian P. Mathematical equations for dental implant stability patterns during the osseointegration period, based on previous resonance frequency analysis studies. Clin Implant Dent Relat Res 2019;21:1028-40.
    PUBMED | CROSSREF

28. Simunek A, Kopecka D, Brazda T, Strnad I, Capek L, Slezak R. Development of implant stability during early healing of immediately loaded implants. Int J Oral Maxillofac Implants 2012;27:619-27.
    PUBMED

29. Lee J, Kim S, Koo KT, Seol YJ, Cho HJ, Lee YM. Histologic analyses of immediate implant placement in infected and noninfected sockets: an experimental pilot study in beagle dogs. Int J Oral Maxillofac Implants 2019;34:575-84.
    PUBMED | CROSSREF

30. Calvo-Guirado JL, López-López PJ, Mate Sanchez JE, Gargallo Albiol J, Velasco Ortega E, Delgado Ruiz R. Crestal bone loss related to immediate implants in crestal and subcrestal position: a pilot study in dogs. Clin Oral Implants Res 2014;25:1286-94.
    PUBMED | CROSSREF

31. Soto-Peñaloza D, Caneva M, Viña-Almunia J, Martin-de-Llano JJ, García-Mira B, Peñarrocha-Oltra D, et al. Effect on osseointegration of two implant macro-designs: a histomorphometric analysis of bicortically installed implants in different topographic sites of rabbit's tibiae. Med Oral Patol Oral Cir Bucal 2019;24:e502-10.
    PUBMED | CROSSREF